

---

# Effects of calcination temperature and curing time on bending strength and microstructure of hydrothermally treated mordenite products

Lei Zheng<sup>1,2,\*</sup>, Xia Zhou<sup>1,2</sup>, Xinyi Zhang<sup>1,2</sup>

1. School of Energy and Environmental Engineering,

University of Science and Technology Beijing, Beijing 100083, China

2. Beijing Key Laboratory of Resource-oriented Treatment of Industrial Pollutants,  
Beijing 100083, China

zhengl@ustb.edu.cn

---

**ABSTRACT.** This paper probes deep into the hydrothermal solidification of mordenite in an attempt to disclose the effects of the treatment and hydrothermal parameters on the strength and microstructure of products. Through the investigation, it is concluded that the calcination temperature promotes the evaporation of absorbed moisture, the loss of crystallization water, elimination of impurities and the collapse of the crystalline structure. The bending strength of mordenite firstly increased and then declined with the elapse of the curing time. As the calcination temperature grew, the bending strength exhibited a decline. Since the peak bending strength was observed at 12h and under 300°C, the 300°C and 12h were determined as the optimal conditions to eliminate the impurities and ensure the good bending strength (11.5MPa) of the solidified products. The research findings provide new insights into the hydrothermal technology for mordenite solidification.

**RÉSUMÉ.** Dans cet article, le durcissement hydrothermal de la mordenite a été étudié en profondeur, en essayant de révéler les effets du traitement et les paramètres hydrothermaux sur la résistance et la microstructure des produits. L'enquête a permis de conclure que la température de calcination favorise l'évaporation de l'humidité absorbée, la perte d'eau de cristallisation, l'élimination des impuretés et l'effondrement de la structure cristalline. La résistance à la flexion de la mordenite a d'abord augmenté, puis diminué avec le temps de durcissement. Lorsque la température de calcination a augmenté, la résistance à la flexion a diminué. Comme la résistance maximale à la flexion a été observée à 12h et à moins de 300 ° C, les conditions optimales ont été déterminées à 300 ° C et à 12 h pour éliminer les impuretés et garantir la bonne résistance à la flexion (11,5 MPa) des produits solidifiés. Les résultats de la recherche fournissent de nouvelles informations sur la technologie hydrothermale pour la solidification de la mordenite.

**KEYWORDS:** mordenite, hydrothermal treatment, bending strength, microstructure, self-humidity control.

*MOTS-CLÉS: mordenite, traitement hydrothermal, résistance à la flexion, microstructure, contrôle de l'auto-humidité.*

DOI:10.3166/ACSM.42.419-427 © 2018 Lavoisier

## 1. Introduction

China boasts an abundance of zeolite resources. Over 100 zeolite deposits have been found in 21 provinces and over 30 million tons of natural zeolite are being consumed annually across the country (Feng and Peng, 2005). More zeolite is consumed for cement production than any other Chinese industry, for natural zeolite can ensure the volume stability of hardened cement paste. In fact, it has been a decade since zeolite was firstly adopted in China as an admixture for concrete production.

Mordenite is a zeolite mineral with the chemical formula,  $(Ca, Na_2, K_2) Al_2Si_{10}O_{24} \cdot 7H_2O$ . It is one of the six most abundant zeolites and is used commercially. Hashimoto (Hashimoto *et al.*, 2003) found that several kinds of zeolites, including phillipsite, hydroxysodalite and analcime, can be obtained from natural mordenite through alkali hydrothermal treatment. The hydrothermal technology consumes five times fewer energy than the conventional firing process (Balandis and Sinkavichene, 2005), as evidenced by its application in the solidification of Ca-Si-Al-H<sub>2</sub>O, the recycling of bottom and fly ashes into high-performance building materials, and the solidification of blast furnace water-cooled slag (BFWS) under saturated steam pressure (1.56MPa) at 473K for 12h with the addition of quartz (Jing *et al.*, 2006). However, there is no report on the strength development of mordenite during hydrothermal treatment.

In addition, it is known that the hydrothermally treated soil has the ability of self-humidity control, thanks to the nanopores formed during the treatment. The same has been found in the hydrothermal treatment products of other materials. For instance, Maenami *et al.* (2004) confirmed that the flooring produced through hydrothermal solidification of Al-rich inorganic wastes has a smaller variation of temperature and humidity than common flooring. Nevertheless, hardly any scholar has investigated the self-humidity control of hydrothermal solidified mordenite.

Considering the general notion that material treatment and hydrothermal parameters have major impacts on product features (Shan *et al.*, 2011), this paper probes deep into the hydrothermal solidification of mordenite in an attempt to disclose the effects of the treatment and hydrothermal parameters on the strength and microstructure of products. (Nathan, 1987) The research findings shed new light on the solidification mechanism of hydrothermally treated mordenite.

## 2. Methodology

### 2.1. Material

The mordenite sample was sieved to eliminate the particles equal to or greater

than 100 $\mu\text{m}$  in size, and then pretreated through 24h calcination at 300 $^{\circ}\text{C}$ , 600 $^{\circ}\text{C}$  and 900 $^{\circ}\text{C}$ , aiming to reveal the effects of calcination temperature on the products. (Zhang *et al.*, 2000)

The principal element analysis was carried out by Lab Center XRF-1700 X-ray fluorescence spectrometry (Shimadzu, Japan). The results show that mordenite contains the following elements: Si 32.1wt%, Al 7.3wt%, Na 1.7wt%, K 1.6wt%, Fe 1.1wt% and Ca 0.7wt%.

Distilled water and analytical grade chemicals were used in all experiments.

## 2.2. Treatment method

Firstly, the mordenite was mixed manually with  $\text{Ca}(\text{OH})_2$  and distilled water, at the water-to-solid mass ratio of 0.1 and the mordenite-to- $\text{Ca}(\text{OH})_2$  mass ratio of 4. The mixtures were then compacted under 15MPa by uniaxial pressing in a mold (10mm $\times$ 15mm $\times$ 40mm). (Kruger *et al.*, 1989) After demolding, the specimens were treated hydrothermally under the saturated pressure at 180 $^{\circ}\text{C}$ , while the curing time was set to 0h, 4h, 12h and 24h.

## 2.3. Experimental strategy

The thermal behavior of mordenite was examined experimentally by an STA449F3 computerized thermo-balance (NETZSCH, German). Before the experiments, the reactor containing terramycin residues was heated up from 50 $^{\circ}\text{C}$  to 1,000 $^{\circ}\text{C}$  at 10 $^{\circ}\text{C}/\text{min}$  and the hydrothermally treated specimens were dried at 60  $^{\circ}\text{C}$  for 2d. Then, five specimens were tested through a three-point flexural strength experiment using an RTM-500 TENSILON testing machine (A&D Company, Japan). The mean flexural strength of the five specimens was adopted as the final result. Meanwhile, the mineralogical composition of the specimens was analyzed by X-ray powder diffraction (XRD) using a D/Max-B diffractometer (Rigaku, Japan). The XRD parameters were set as follows:  $\text{Cu}(\text{K}\alpha)$  radiation, 40keV accelerating voltage, 80mA current, 5~70 $^{\circ}$   $2\theta$  scanning range, 0.02 $^{\circ}$  step and 6 $^{\circ}\text{min}^{-1}$  scan speed. The specific surface area (SSA) and the pore distribution were measured by the  $\text{N}_2$  gas adsorption through Brunauer–Emmett–Teller (BET) method and Barrett–Joyner–Halenda (BJH) method (ASAP 2010, Micromeritics, USA), while mercury intrusion pore distribution, density and porosity were determined by mercury intrusion porosimetry (Quantachrome, US).

## 3. Results and discussion

### 3.1. Calcination effects

Figure 1 presents the TGs obtained through the thermal behavior experiments in Ar atmosphere. It can be seen that the first mass loss appeared between 50 $^{\circ}\text{C}$  and

200°C, which is attributable to moisture evaporation. The evaporation released the crystal water, which in turn caused the dehydration reactions. The second mass loss occurred between 200°C and 600°C due to the elimination of impurities in micropores. After the temperature surpassed 600°C, other compounds with relatively strong chemical bonds degraded, leading to a slow mass loss.

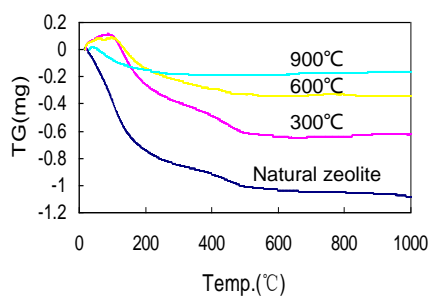


Figure 1. Thermo-gravity (TG)-temperature curves

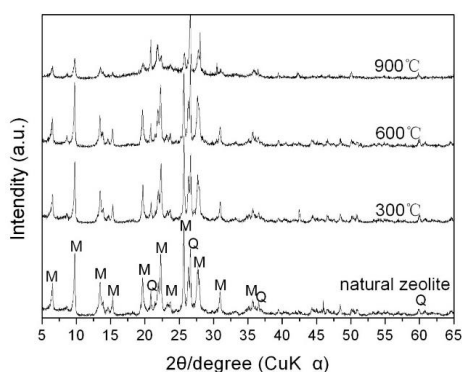


Figure 2. XRD pattern of mordenite calcined at different temperatures (M: mordenite; Q: quartz)

The XRD pattern of mordenite calcined at different temperatures is shown in Figure 2. It is clear that the collapse of crystalline structure propagated with the growing calcination temperature, which agrees well with the SEM results in Figure 3. According to the SEM patterns on compacted specimens without hydrothermal treatment, the specimen synthesized from natural mordenite had a heavy presence of

impurities in micropores, that synthesized from mordenite calcined at 300°C carried no impurity in micropores, while that synthesized from mordenite calcined at 900°C suffered from the collapse of crystalline structure.

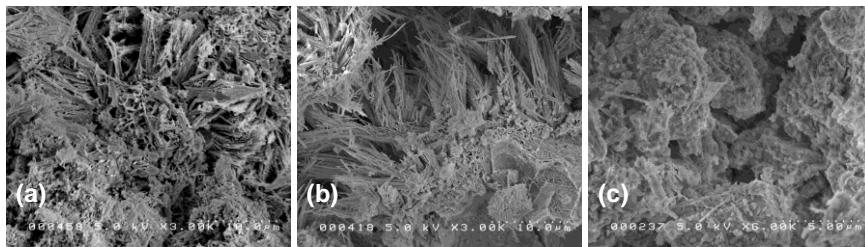


Figure 3. SEM patterns of compacted specimens without hydrothermal treatment, synthesized from (a) natural mordenite, (b) mordenite calcined at 300°C and (c) mordenite calcined at 900°C

### 3.2. Strength performance

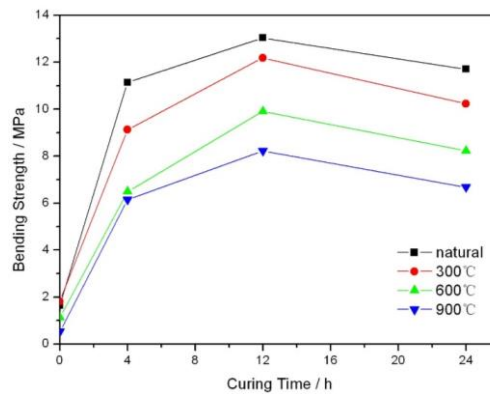


Figure 4. Curing time-bending strength curves

As shown in Figure 4, the bending strength of the specimens was controlled by both calcination temperature and curing time. With the elapse of curing time, the strength firstly increased and then decreased. The peak bending strength was observed at 12h. As the calcination temperature grew, the bending strength exhibited a decline.

The XRD results in Table 1 shows that the C-S-H gradually transformed into tobermorite as the reaction went on. (Hong and Glasser, 1999)

Considering the above, 300°C and 12h are the optimal conditions to eliminate the impurities and ensure the good bending strength (11.5MPa) of the solidified products. The strength value exceeds the level required for building materials like tiles and bricks.

*Table 1. XRD results on the main synthesis products at 180°C (C: C-S-H; T: tobermorite)*

Calcination temperature	Reaction time (h)		
	4h	12h	24h
Natural mordenite	C	C, T	C, T
300°C	C	C, T	C, T
600°C	C, T	C, T	C, T
900°C	C, T	T	T

### 3.3. Pore structure performance

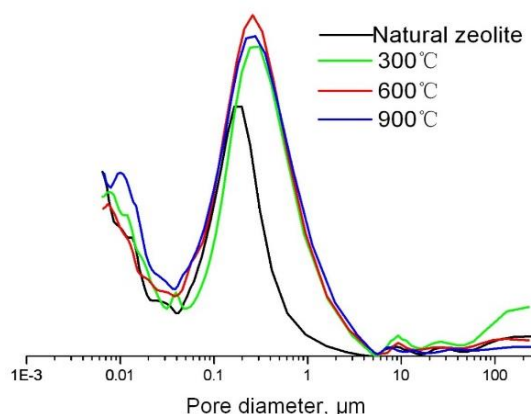


*Figure 5. Pore size distribution of specimens synthesized from different mordenites after 4h curing*

Figure 5 illustrates the pore size distribution of specimens synthesized from different mordenites after 4h curing. According to the International Union of Pure and Applied Chemistry (IUPAC), the pores with diameter between 200 and 50nm are macropores, those with diameter between 50 and 3.6nm are mesopores, and those with diameter smaller than 3.6nm are micropores.

At the start of the hydrothermal reaction, macropores existed in the gaps between unreacted particles. As the reaction proceeded, the newly formed chemicals bridged the gaps, causing a decline in macropore volume and the formation of mesopores and micropores. The latter two types of pores mainly originated from the pores within the network of newly formed chemical network (Zheng *et al.*, 2016; Zheng *et al.*, 2015). When mordenite was calcined at 300°C, the solidified specimen had a high pore volume, which is reasonable because calcination eliminates impurities in pores. However, when the calcination temperature rose to 600 or 900°C, the pore structure was similar to that under 300 °C, indicating that 300 °C is sufficient for impurity removal.

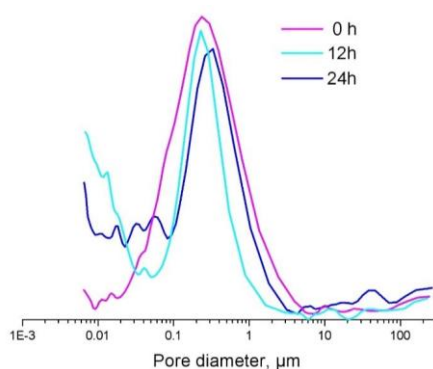


Figure 6. Pore distribution of specimens synthesized from natural mordenite

When the curing time increased to 12h, more and more tobermorite phases were formed (Table 1). This means the macropore dominance in the microstructure (the 0h curve in Figure 6) is overthrown by mesopores and micropores (the 12h curve in Figure 6), which explains the strength enhancement at 12h.

Compared with the specimen after 12h curing, the specimen after 24h curing saw a decrease in the volume of mesopores and micropores and a shift to macropores. This trend may be caused by the growing size of tobermorite crystals after curing for 24h (Figure 7). The size growth led to the change in pore distribution, and thus weakened the bond in the matrix. This is consistent with the results on bending strength.

The previous studies have shown that the self-humidity control ability hinges on the mesopores with the diameter between 4 and 20nm and the condensation of moisture in the capillary pores can be estimated by the Kelvin's equation. In our test system, the self-humidity control ability of the specimens may arise from the pores developed in the formation of tobermorite. As shown in Figure 6, the specimen after 12h curing had the highest mesopore volume, and thus the optimal ability of self-humidity control.

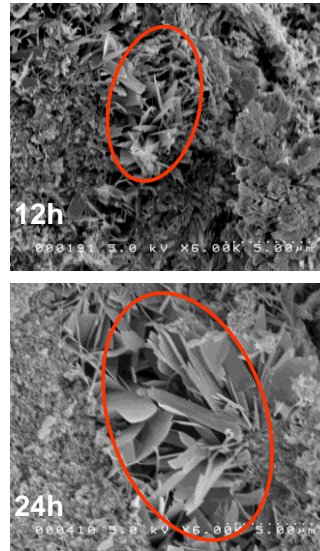


Figure 7. SEM patterns of the specimens synthesized from natural mordenite

#### 4. Conclusions

This paper explores the effects of calcination temperature and hydrothermal curing time on the bending strength and pore structure of mordenite. The main conclusions are as follows.

The calcination temperature promotes the evaporation of absorbed moisture, the loss of crystallization water, elimination of impurities and the collapse of the crystalline structure. The bending strength of mordenite firstly increased and then declined with the elapse of the curing time. As the calcination temperature grew, the bending strength exhibited a decline. Since the peak bending strength was observed at 12h and under 300°C, the 300°C and 12h were determined as the optimal conditions to eliminate the impurities and ensure the good bending strength (11.5MPa) of the solidified products

The future research will further compare the self-humidity control ability between the natural mordenite and the products of mordenite hydrothermally treated under even more diverse conditions.

#### References

- Balandis A., Sinkyavichene I. (2005). Hydrothremal synthesis of leucite and its application in engineering ceramics. *Glass and Ceramics*, Vol. 62, No. 1-2, pp. 21-24. <https://doi.org/10.1007/s10717-005-0031-3>

- Feng N. Q., Peng G. F. (2005). Applications of natural zeolite to construction and building materials in China. *Construction and Building Materials*, Vol. 19, No. 8, pp. 579–584. <https://doi.org/10.1016/j.conbuildmat.2005.01.013>
- Hashimoto T., Watanabe Y., Moriyoshi Y., Yamada H., Minato J., Sekita M., Tanaka J., Komatsu Y. (2003). Modification of natural mordenite by alkali hydrothermal treatments. *J. Ion. Exchange.*, Vol. 14, pp. 125-128.
- Hong S. Y., Glaser F. P. (1999). Alkali binding in cement pastes Part I. The C-S-H phase. *Cement and Concrete Research*, Vol. 29, No. 12, pp. 1893-1903. [https://doi.org/10.1016/S0008-8846\(99\)00187-8](https://doi.org/10.1016/S0008-8846(99)00187-8)
- Jing Z., Ishida E. H., Jin F., Hashida T., Yamasaki N. (2006). Influence of quartz particle size on hydrothermal solidification of blast furnace slag. *Ind. Eng. Chem. Res.*, Vol. 45, pp. 7470-7474.
- Kruger M. B., Jeanloz R., Williams Q. (1989). Vibrational spectra of  $Mg(OH)_2$  and  $Ca(OH)_2$  under pressure. *The Journal of Chemical Physics*, Vol. 91, pp. 5910. <https://doi.org/10.1063/1.457460>
- Maenami H., Isu N., Ishida E. H. (2004). Solidification of Al-rich inorganic waste material using hydrothermal technology. *Journal of the ceramic society of Japan*, Vol. 112, No. 5, pp. 1316-1322.
- Nathan C. F. (1987). Secretory products of macrophages. *The Journal of Clinical Investigation*, Vol. 79, No. 2, pp. 319-326. <https://doi.org/10.1172/JCI112815>
- Oida M., Maenami H., Isu N., Ishida E. H. (2004). Recycling of inorganic waste as paving tile by hydrothermal technology. *Journal of Ceramic Society of Japan*, Vol. 112, No. 5, pp. 1368-1372. <https://doi.org/10.14852/jcersjsuppl.112.0.S1368.0>
- Shan C., Jing Z., Pan L., Zhou L., Pan X., Lu L. (2011). Hydrothermal solidification of municipal solid waste incineration fly ash. *Journal of the Ceramic Society of Japan, Supplement*, Vol. 37, No. 2-5, pp. 551-565. <https://doi.org/10.14852/jcersjsuppl.112.0.S1316.0>
- Zhang Q. H., Gao L., Guo J. K. (2000). Effects of calcination on the photocatalytic properties of nanosized  $TiO_2$  powders prepared by  $TiCl_4$  hydrolysis. *Applied Catalysis B Environmental*, Vol. 26, No. 3, pp. 207-215. [https://doi.org/10.1016/S0926-3373\(00\)00122-3](https://doi.org/10.1016/S0926-3373(00)00122-3)
- Zheng L., Wang W., Gao X. (2016). Solidification and immobilization of MSWI fly ash through aluminate geopolymerization: Based on partial charge model analysis. *Waste Management*, Vol. 58, pp. 270-279. <https://doi.org/10.1016/j.wasman.2016.08.019>
- Zheng L., Wang W., Qiao W., Shi Y., Liu X. (2015). Immobilization of  $Cu^{2+}$ ,  $Zn^{2+}$ ,  $Pb^{2+}$ , and  $Cd^{2+}$  during geopolymerization. *Frontiers of Environmental Science & Engineering*, Vol. 9, No. 4, pp. 642-648. <https://doi.org/10.1007/s11783-014-0707-4>

